In Situ Observations of the Microphysical Properties of Young Cirrus Clouds**

J. STRÖM,* B. STRAUSS,+ T. ANDERSON,# F. SCHRÖDER,+ J. HEINTZENBERG,@ AND P. WENDLING+

*Department of Meteorology, Stockholm University, Stockholm, Sweden
+Deutsche Forschungsanstalt für Luft- und Raumfhart, Institute für Physik der Atmosphäre, Oberpfaffenhofen, Germany
#Joint Institute for the Study of the Atmosphere and Ocean University of Washington, Seattle, Seattle, Washington
@Institute for Tropospheric Research, Leipzig, Germany

(Manuscript received 8 July 1996, in final form 7 March 1997)

ABSTRACT

In situ measurements made in cold (−35° to −60°C) cirrus clouds over southern Germany in March 1994 are presented. The clouds appeared to be in an early stage of their life cycle and their properties in many ways resemble those reported for ice fogs. Crystal concentrations were high (median 2.5 cm^{-3}, STP) and sizes small with a diameter of mean mass of typically 16 μm. The cloud on 18 March presents an interesting case for modeling studies of cirrus formation. On that particular day, the bulk properties of the cloud appeared to be connected to wave structures in the vertical wind field consistent with the Brunt–Väisälä frequency, which gave a corresponding wavelength of 40–50 km. Furthermore, analyses of potential temperature and vertical wind suggested that the vertical displacement producing these clouds was less than 100 m. Size distribution measurements of interstitial particles and crystal residues (particles remaining after evaporation of the crystals) show that small aerosol particles (diameters <0.5 μm) participate in the nucleation of cirrus crystals at low temperatures. Because the aerosol in this small size range is readily perturbed by anthropogenic activity, it is important to study the link between upper tropospheric aerosol properties and cirrus cloud microphysics. While the observations presented here are not adequate to quantify this link, they pave the way for modeling studies and would be interesting to compare to cirrus observations from cleaner regions.

1. Introduction

The net radiative effect of a cirrus cloud may be either to warm or cool the earth, depending on the balance between its solar albedo and its thermal emittance. Since this balance depends strongly on cloud water content, crystal shape, and crystal size distribution (Stephens et al. 1990), it is important to understand the processes that control these properties. The nucleation process of ice crystals can be divided into spontaneous freezing of supercooled haze droplets, sometimes referred to as homogeneous crystal formation, and heterogeneous crystal formation. The heterogeneous process refers to water vapor freezing on particles particularly favorable for ice crystal formation, or through contact or immersion freezing. In a modeling study, DeMott et al. (1994) showed that cloud properties critically depended on the assumptions made regarding the properties of the aerosol. This implies that perturbations of the ambient aerosol, natural or anthropogenic, can alter the occurrence and properties of cirrus clouds and thus potentially climate. To be able to predict the response of cirrus clouds to a change in aerosol characteristics, a more in-depth understanding about the processes of formation and early development of cirrus clouds is required. This knowledge will also be useful in improving parameterizations of cirrus clouds used in forecast models. With the exception of process models, ice clouds are often treated with schemes developed for warm clouds. The criteria for cloud formation in a grid box are primarily determined by the convergence of water vapor and a humidity threshold. Consideration is seldom given to the stochastic nature of ice formation, nor to the fact that cirrus clouds can be sensitive to small-scale variations in the wind field within a grid box.

Wave cloud measurements by Heymsfield and Miloshevich (1993, 1995) constitute the most extensive study to date of cirrus formation processes. These authors concluded the spontaneous freezing of solution droplets plays an important role in the initial ice formation in cirrus, and at temperatures below −51°C the particles serving as cloud condensation nuclei (CCN) were composed of sulfates other than ammonium sulfate. However, the vertical velocities in these clouds were on the order of meters per second and the air parcel was lifted 1 km from the base level, which resulted in a cooling of the air by ~10 K. In the more horizontally

** Joint Institute for the Study of the Atmosphere and Ocean Contribution Number 395.

Corresponding author address: Dr. Johan Ström, Department of Meteorology, Stockholm University, S-106 91 Stockholm, Sweden. E-mail: johan@misu.su.se

extended frontal cirrus, the vertical velocities and thus cooling rates are expected to be much lower.

This paper presents in situ measurements of cirrus clouds in which the vertical wind speeds are more typical for synoptic-scale cirrus and an order of magnitude less than in wave clouds. The analyses focus on a flight conducted on 18 March 1994 over southern Germany from which measurements of ambient aerosol, thermodynamic, microphysical, and cloud residual properties are presented. The observed properties from this case are suitable for input and comparison to model simulations. In addition to the case study, cloud properties observed during three other flights made on other days but in the same area and under similar atmospheric conditions are also presented.

2. Experimental

In situ measurements in cirrus clouds with aerosol instrumentation and cloud probes were conducted during four flights on 18, 22, and 25 (two flights) March 1994. These missions were flown mainly over southern Germany in a sector roughly bounded by latitude 47°N and 50°N, and longitude 11°E and 15°E. During the measurement period, the synoptic weather over central Europe was such that in the free troposphere the airflow was from west or northwest except on 22 March when a ''cutoff low'' over France disturbed the flow pattern. In this case the air flow was from the north over the measuring area. On 23 March, the wind pattern was restored again to a westerly air flow.

Instruments

All instruments were operated on board the Deutsche Forschungsanstalt für Luft- und Raumfhart Falcon research aircraft. The Falcon instrumentation for meteorological data uses the following instruments (Schumann et al. 1995): Temperature is measured with Rosemount Pt100 and Pt500 sensors with 0.01 K resolution and ± 0.5 K accuracy. Static pressure is measured by a Rosemount 1201F1 pressure transducer with absolute accuracy ± 1.2 hPa. Wind components are measured using a five-hole pressure probe at the tip of a nose boom and inertial navigation system. This resolves velocity fluctuations to better than 0.03 m s^{-1}. Humidity was measured by a cryogenically cooled frostpoint mirror (CR-1) (Busen and Buck 1993; Ström et al. 1994a). The response time of the instrument ranges from about 5 to 30 seconds depending on the frostpoint, and the dew- or frostpoint readout accuracy is ± 0.3 K. The accuracy of the frostpoint and ambient temperature measurements results in an absolute uncertainty of the calculated average relative humidity of about $\pm 10\%$.

Two different PMS (Particle Measuring Systems) cloud probes mounted on wing pods were carried onboard the aircraft: a two-dimensional optical array probe (PMS 2D-C) (Knollenberg 1970) to obtain information about crystals with dimensions between 50 and 800 μm, and a forward-scattering spectrometer probe (FSSP-100) to size particles in the range 2–32 μm (Dye and Baumgardner 1984). After the flights it was found that the FSSP instrument had a faulty laser and the data from this probe was excluded.

Another instrument to measure crystal size distribution and habit working on a completely different physical principal is the ice replicator, designed and built by J. Hallett (Desert Research Institute). This device is built into the same type of wing pod as the PMS probes. A 16-mm celluloid film coated with a chloroform formvar solution is exposed to the ambient air through a small (2 mm $\times$ 7 mm) slit facing the flight direction. This opening results in a sampling rate of 2.5–3 L s^{-1}, depending on airspeed. Cloud particles that enter the slit and impact on the film leave a replica of their shape in the formvar. Due to problems with the Formvar coating, it was necessary to manually select those portions of the film suitable for analysis. The selected portions were then evaluated automatically using pattern recognition software. The collection efficiency of the replicator has not been calibrated; hence its sampling characteristics are not well known for particles smaller than approximately 10-μm diameter. However, simple calculations, assuming impact on a long cylinder, yield a 50% sampling efficiency of around 4-μm diameter. The upper detection limit is mainly determined by the breakup of large crystals as they impact on the film, which causes difficulties in data interpretation. This problem becomes significant for particles with dimensions larger than 100 μm. For more information about the replicator refer to Hallett (1976).

Two complementary inlets were used to obtain information about the partitioning of aerosol particles within the clouds. These are the Counterflow Virtual Impactor (CVI) or supermicrometer inlet, and the interstitial inlet or submicrometer inlet. The submicrometer inlet is a ¼ inch stainless steel tube that is tapered to give an effective opening cross section of 3.8 mm^2. The opening of the inlet is turned opposite to the flight direction, which results in cloud particles not being sampled due to their inertia carrying them past the inlet. Thus, only the interstitial aerosol (unactivated particles in between the cloud elements) will be sampled. The upper cutoff for this inlet is estimated to be just under 1-μm aerodynamic diameter (Schröder and Ström 1997). The CVI is a device that inertially separates cloud elements larger than a certain aerodynamic size from the surrounding atmosphere into warm, dry, and particle-free air (Ogren et al. 1985). Water vapor and residue particles left behind by the evaporated cloud elements are subsequently sensed and sampled by instruments downstream of the CVI. The device has been used in several airborne experiments as well as on the ground (e.g., Noone et al. 1992; Twohy et al. 1989). The lower cutoff size of the CVI, in terms of aerodynamic diameter, is determined by the true air speed and the dimensions

of the CVI probe. Ground-based calibrations and detailed numerical modeling of this device show that the sampling characteristics can be predicted accurately by rather simple formulations (Noone et al. 1988; Anderson et al. 1993; Lin and Heintzenberg 1995). The calculated 50% sampling efficiency for the probe used in this experiment is 4.5-μm diameter.

The evaporating cloud particles must pass a 90° bend in the sampling tube before they enter the aircraft. In previous airborne versions of the CVI, any cloud particle not fully evaporated and with enough inertia could hit the inside wall of the back of the probe sample tube. To better characterize the sampling properties of the probe used in this study, it has been equipped with a second virtual impactor in the 90° bend. The sample flow and geometry are designed such that particles larger than 50-μm aerodynamic diameter are collected by this second virtual impactor and thereby excluded from the analyses.

Inside the aircraft, the sample air from the two inlets is distributed to different sensors. The concentration of ambient aerosol and residual particles larger than 0.018-μm diameter was measured by two TSI-3760 condensation particle counters modified for aircraft use (Schröder and Ström 1997). Residual particles are nonvolatile material remaining after evaporation of the condensed water from the cloud particles. Assuming that each cloud element (crystal or water drop) leaves behind only one residue particle, these measurements yield an equivalent number concentration for cloud particles having an aerodynamic diameter larger than the lower cut size of the CVI. The size distribution of the sampled aerosol and residual particles between 0.1 and 3.5 μm diameter was measured by a PMS PCASP (Passive Cavity Aerosol Spectrometer) working alternatively on both inlets. A dual-beam Lyman-α hygrometer (Zuber and Witt 1987) was used to measure the evaporated water from the sampled cloud element, which corresponds to the condensed water content (CWC) in cloud particles larger than the lower cut size of the CVI.

3. Results and discussion

Unless stated otherwise, all values are reported as 3-s averages (corresponding to a horizontal resolution of 500–600 m) and concentrations are normalized to standard temperature and pressure (STP) (273.15 K and 1013.25 hPa) values. Due to the low temperatures observed in cirrus, cloud particles entering the CVI are almost certainly frozen and will thus be referred to as crystals.

a. Flight on 18 March 1994

The flight path on 18 March is shown in Fig. 1. The first part of the flight was conducted over the Alps in virtually cloud-free air. After three flight legs over the Alps, the aircraft flew east and then turned north-northwest almost directly into the wind. The aircraft entered a cirrus cloud at 8800-m pressure altitude (top level) marked as A in Fig. 1. After two descents to 8500 m (middle level) at about 1136 UTC (B) and 8200 m (bottom level) at about 1144 UTC (C), the aircraft finally exited the cloud 1156 UTC at point (D). The average temperatures on these levels were −53.3, −51.2, and −48.8°C, respectively. Shortly after leaving the cloud, the aircraft turned to a southwesterly direction and descended towards Oberpfaffenhofen (near Munich). During the descent the aircraft passed through a less dense cloud layer between 7 and 8 km. From an altitude of about 4500 m and down to the boundary layer, the aircraft was inside a nimbostratus cloud. The data from the three levels inside clouds are presented in Figs. 2 and 3.

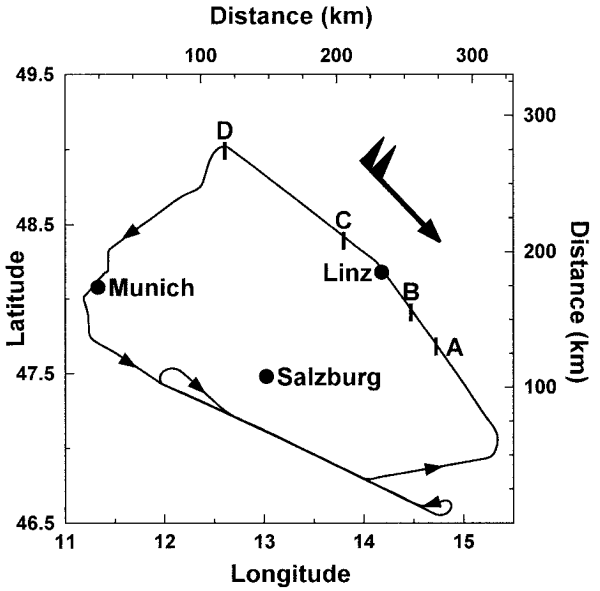

FIG. 1. Flight track on 18 March 1994. The letters A–D indicate where the aircraft made descents; the large arrow shows the prevailing horizontal wind and the small arrows show flight direction.

As the aircraft approached the cirrus cloud on the top level, the relative humidity increased from near ice saturation to near water saturation. The crystal concentration and CWC did not show a significant increase until RH_w (relative humidity over water) had reached about 80% around 1134 UTC. At that time the concentrations were about 1 cm^{-3} and 1 mg m^{-3}, respectively. On the middle level, crystal concentrations ranged between 0.5 and 4.5 cm^{-3}, and CWC ranged between 1 and 6 mg m^{-3}. The highest values were observed on the bottom level for both crystal concentration (2–13 cm^{-3}) and CWC (5–30 mg m^{-3}). The flight leg average RH_w increased from 95% to a slightly higher value of 98% between the middle and bottom level. Over the distance of a flight leg, the artificial oscillations made by the frostpoint hygrometer are averaged out. Nevertheless, at the observed temperatures in the cloud of about

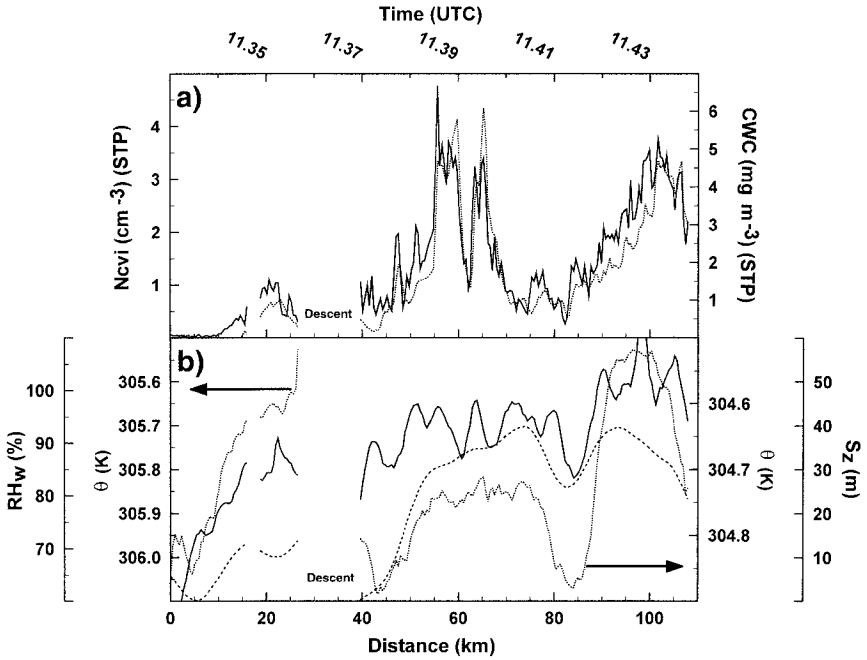

FIG. 2. Measurements from the top and middle level in cirrus cloud on 18 March 1994 as a function of distance and time. (a) Number of crystals (solid line) and cloud water content (dotted line) as measured by the CVI. (b) Relative humidity over water (solid line), vertical component of trajectory calculated from measured vertical velocity (dashed line), and potential temperature (dotted line). Note the two different scales for potential temperature. The gaps in this figure occur when the OPC is switched between CVI and interstitial sample flow.

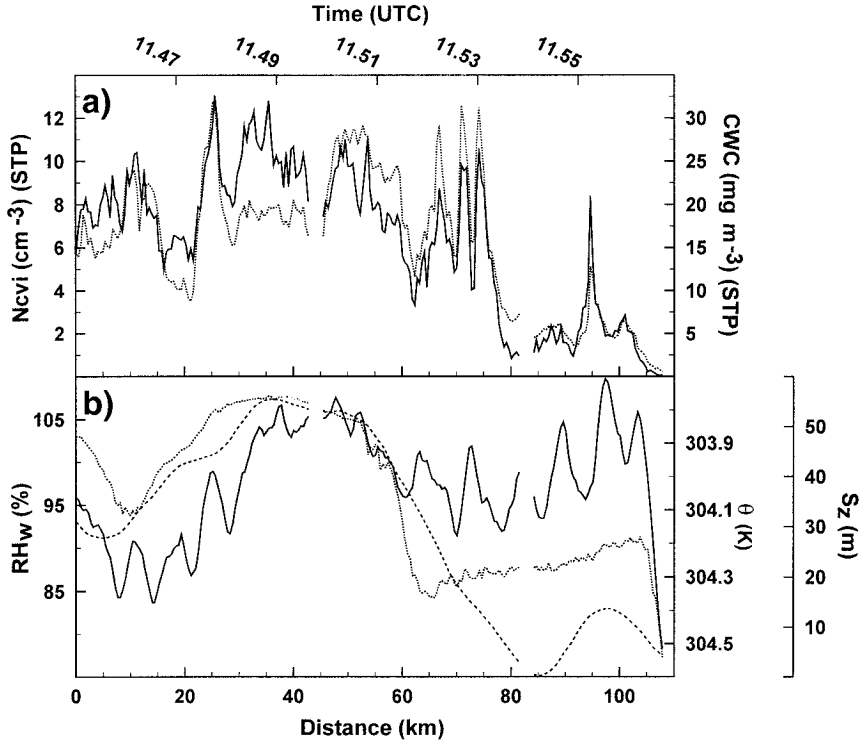

FIG. 3. As in Fig. 2 but for the bottom level.

−50°C, the observed humidities are still well above ice saturation. Low temperatures and humidities near water saturation, together with the assumption that the aerosol is dominated by water soluble material in the tropopause region, imply that most particles have gone through a liquid phase before nucleating ice. However, it is not possible to determine whether these droplets include inclusions or impurities that may stimulate the freezing process.

A very important feature in cloud formation is the dynamic forcing, that is, vertical motion and turbulence. In process studies, a Lagrangian experiment where one can follow an air parcel and observe how dynamics, thermodynamics, and microphysics interact (over time) would be optimum. This type of approach is very difficult to accomplish with an aircraft. Heymsfield and Miloshevich (1993) circumvented the problem by flying in several levels in a lenticular cloud, and due to the persistent wind pattern in the cloud they could make a composite picture and put the measurements into a Lagrangian perspective. One advantage with aircraft measurements, on the other hand, is that one can cover long distances in a relatively short time period. If one assumes that the measurements represent a snapshot in time, it is still possible to obtain information about the dynamic forcing in the cloud by retrieving the vertical component of the trajectories using the measured vertical wind speed as suggested by Ström and Heintzenberg (1994). Since the vertical wind speed (w) is merely the time derivative of the vertical displacement of an air parcel, one can integrate the vertical wind speed along the horizontal wind to recreate the vertical component of the air parcel trajectory, S_z, an indicator of relative vertical displacement:

$$S_z = \int_{t_0}^{t} w\, dt. \tag{1}$$

In order to do this, the flight path must be aligned with the horizontal wind, which is more or less the case for the flight on 18 March (between A and D in Fig. 1), where the aircraft heading was within about ±5° of the wind direction. Furthermore, the measured vertical wind speed is assumed to be representative over a sufficient vertical depth (~100 m). One other approach to get information about the dynamic forcing is to study the variation in potential temperature along the flight track. Assuming only adiabatic processes, the temperature deviation around a mean is inversely proportional to the vertical motion of an air parcel. For an aircraft flying at a constant altitude, the air coming from above will be warmer than the mean temperature and the air coming from below will be colder than the mean temperature. A 30-m change in altitude for an air parcel corresponds to a change in temperature of approximately 0.3 K. Both the observed potential temperature θ and S_z (calculated from wind data as described above) are presented in Figs. 2b and 3b.

The two parameters show variations in altitude and temperature that are consistent with each other. Note that latent heat release, which would induce temperature changes on the order of 10^{-2} K, is negligible compared to the observed temperature variations. The time series of evident anticorrelation between θ (note the inverted scale) and S_z suggests that the dynamic forcing was due to wave structures in the vertical wind field with an amplitude of 25–50 m. From the middle and bottom flight levels an apparent wavelength of 40–50 km is estimated. With a horizontal wind speed of about 50 m s^{-1}, measured by the Falcon aircraft, this yields a period of about 15 min. The measured lapse rate of 0.78 K/100 m yields a Brunt–Väisälä period for this part of the atmosphere of between 12 and 13 min, similar to the estimate from Figs. 2 and 3. Moreover, this apparent wave pattern fits well with the scales of ''mesoscale generating regions'' observed by Sassen et al. (1989). Note that the wave structures observed on 18 March are very different from those found in classic wave clouds as studied by Heymsfield and Miloshevich (1993). Despite oscillations induced by the instrument, the RH_w signal displays a trend similar to those of θ or S_z. At ambient conditions, a 0.3 K change in temperature corresponds to about 3% change in relative humidity. There is also a significant correlation between the number of crystals N_{cvi}, and both θ and S_z. On the bottom level (Fig. 3), N_{cvi} and S_z were correlated with an r^2 of 0.79, while N_{cvi} and θ were anticorrelated with an r^2 of 0.87.

The 2D probe did not observe enough crystals to be able to calculate a useful concentration during any part of the cloud penetration. This implies that crystal sizes did not exceed 50-μm diameter (the upper cut size of the CVI). Therefore, the CVI sampled all the ambient crystals larger than its lower cut size of 4.5-μm diameter. The diameter of mean mass (DMM), defined as the cube root of $(CWC/N_{cvi})(6/\pi)$, varies between 10 and 20 μm with an increase toward lower altitudes. The crystal size distributions deduced from replicator data appear to be grouped into two regimes, shifted to larger and smaller sizes, respectively. The size distributions from these subjectively divided groups are presented in Fig. 4 as envelopes of one standard deviation above and below the mean. The number mode in both cases is associated with crystals smaller than 10-μm diameter. For crystals larger than about 15 μm the average slopes of the distributions become less steep, which results in a bimodal volume distribution. This could be an indication of mixing of air from different regions of the cloud or of multiple nucleation events. In the latter case, a few crystals were first formed and had time to grow before a second and stronger event produced many crystals, which then have to be smaller due to the limited water vapor supply. However, one should keep in mind that the uncertainty is largest in this size range above 15 μm due to poor counting statistics. The effective diameters calculated from the average size distributions are 8 μm (solid line) and 12 μm (dotted line). Using

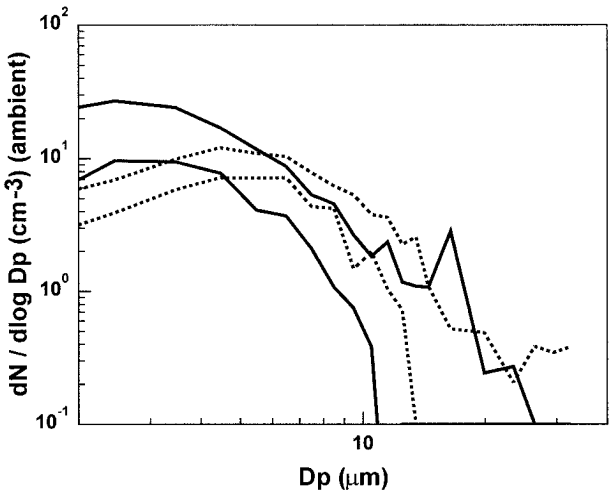

FIG. 4. Crystal size distribution as measured by the replicator. The envelope shows the arithmetic mean plus/minus one standard deviation. The solid and dotted line represents two observed regimes (see text for details).

only the part of the size distribution that is below 15 μm, the effective diameters are 6 and 8 μm, respectively. The effective diameter is the integral of the third moment of the crystal size distribution divided by the integral of its second moment.

The smallest crystals are mostly irregular (potato shaped) spheroids, a crystal habit termed droxtals by Thuman and Robinson (1954). According to Ohtake (1970), this shape is attributed to the fast freezing of haze droplets, which does not allow for the development of normal hexagonal and rectangular faces. With increasing crystal size the shapes become more and more hexagonal, and plates, columns, and bullet rosettes were observed for the largest crystals (20–30 μm). It is interesting to note that replicas of ice-fog crystals made in Alaska (Ohtake 1970) appear almost identical to those made during this experiment in cirrus clouds. An example of replicas from the flight on 18 March is shown in Fig. 5. The sampled volume corresponds to about 1 L ambient air. Even the ice-fog size distributions show striking similarities with those presented in Fig. 4. In both cases, the number modes are located between 5 and 10 μm diameter.

Several features of the above measurements suggest that the cloud on 18 March was in its developing stage. First, the cloud consisted of numerous small crystals with no crystals larger than 50 μm. Second, the humidity was considerably above ice saturation at all times. In a well-aged cloud one would have expected the humidity to have dropped back to near ice saturation, while the size distribution would have shifted toward larger sizes than those observed. Finally, N_{cvi} and CWC display a strong correlation with vertical displacement (as indicated by either θ or S_z), suggesting a direct microphysical response to a dynamic forcing.

In young cirrus, where processes like coagulation and aggregation are of little importance, the residual particle that remains after evaporating a crystal is assumed to

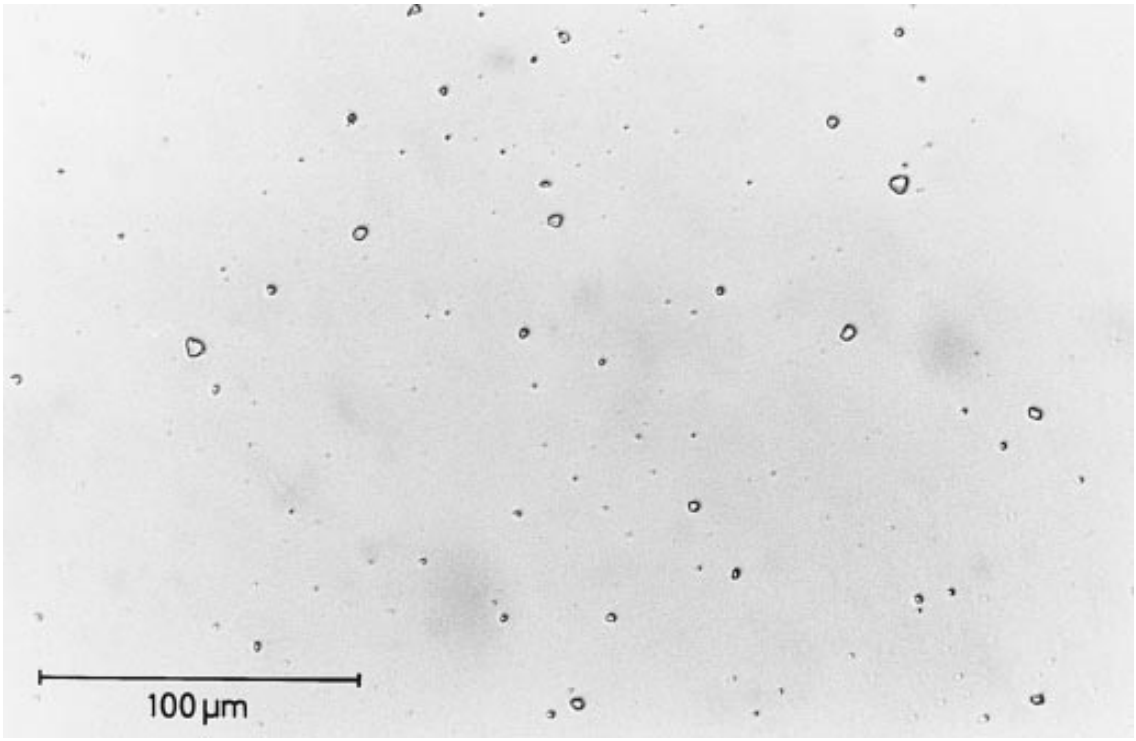

FIG. 5. An example of crystal replicas from the flight on 18 March 1994.

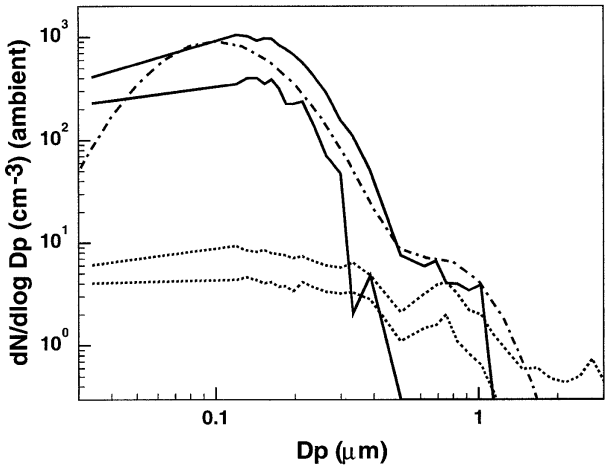

FIG. 6. Average size distributions of interstitial aerosol and cloud residues, shown as solid and dotted lines, respectively. The envelopes show the arithmetic mean plus/minus one standard deviation. The dash-dotted line is the sum of two lognormal distributions, fitted to the sum of the interstitial and residual aerosol size distribution. The fitted curve has the parameters $N_1 = 350$ cm^{-3}, $N_2 = 1$ cm^{-3}, $Dg_1 = 0.1$ μm, $Dg_2 = 0.725$ μm, $\sigma_1 = 1.65$, and $\sigma_2 = 1.4$.

be the same as that upon which the crystal first nucleated. Thus, the residual size distribution represents the part of the ambient aerosol that took part in cloud formation. Figure 6 shows 2-min averages of the residual and interstitial size distributions from a denser part of the cloud taken between 1145 and 1151 UTC. Because the payload only carried one PCASP instrument, the averages had to be performed sequentially. Average crystal concentration, CWC, and interstitial aerosol concentration differed less than 20% between the two averaged periods. Figure 6 also shows the sum of two lognormal curves as a fit to the total aerosol distribution. The total aerosol distribution is taken as the sum of the interstitial and residual size distributions.

The concentration of residual particles has a number mode around 0.1 μm and a local maximum at about 0.7-μm diameter. The latter maximum was also observed in cirrus measurements made over the North Sea (Ström et al. 1994b). However, a second peak in the residue distribution around 0.35-μm diameter observed over the North Sea was not found in present study. The measurements over the North Sea were made in clouds with less CWC and fewer but larger crystals. It is possible that size separation of crystals due to gravitational settling, processes not likely to be very important on 18 March, caused the observed variations in the residue size distribution over the North Sea. Jensen et al. (1994) argued on theoretical grounds that aerosol particles smaller than 0.6-μm diameter do not significantly affect ice nucleation in midlatitude cirrus. Measurements presented in this paper and those from the North Sea (Ström et al. 1994b; Noone et al. 1993) do not support this conclusion. More than 90% of the residual particles were smaller than 0.6 μm in the cloud discussed here. This is also the case for ice-fog nuclei as observed in Ohtake (1970).

An interesting observation, consistent with the freezing of solution droplets as the crystal nucleation mechanism, is that the shape of the residual size distribution changed very little with total crystal concentration (or, indeed, with any other parameter). The probability per unit time that a solution droplet will freeze obeys a power law dependence on dry particle size (DeMott et al. 1994), under the assumption that particle chemistry is constant with size. The slope of this probability function (vs particle size) depends weakly on changes in humidity and temperature and will thus be essentially the same at all times and locations within the investigated clouds at a given flight level. Assuming that crystal nucleation does not deplete a significant fraction of the particles at a given size, the slope of the scavenging efficiency curve will be the same as the slope of this probability function. Put another way, the freezing probability for a solution droplet formed on a 0.1-μm particle is much lower than for a solution droplet formed on a 0.5-μm particle; however, the ratio of these probabilities will be essentially constant with time. Therefore, if the ratio of interstitial particles at these two sizes remains constant, the ratio of crystal-nucleation rates for these two sizes will also remain constant. Thus, although our measurements correspond to different times within the cloud formation process, we would expect the shape of the residual size distribution to be constant, as long as the ambient aerosol size distribution was constant as well.

The measurements presented here allow size-dependent scavenging efficiency to be calculated as the ratio of residual to total particles at a given size, where total particles means the sum of residual and interstitial particles. This scavenging efficiency is plotted in Fig. 7 along with the fitted function

$$f(d) = \arctan\left(\frac{\left(\frac{d}{d_{50}}\right)^5}{\frac{\pi}{2}}\right) + 0.0085, \qquad (2)$$

where $d_{50} = 0.53$ μm. The correlation to the data for this function (solid line in Fig. 7) is 0.997. Figures 6 and 7 show that although the scavenged fraction of sub-0.3-μm particles is small, they may dominate the residual particles in absolute number. Due to the shape of the efficiency curve, many features of the residual size distribution are determined by the shape of the ambient aerosol distribution.

In Fig. 7 the form of the scavenging efficiency curve is compared with a parameterization of the probability of freezing per unit time as given in DeMott et al. (1994). At a temperature of -49°C (the observed temperature), the best fit to the data is obtained for an RH_w value of 94.9%. Using a curve at a lower RH_w (in effect moving the curve to the right in the figure) and letting

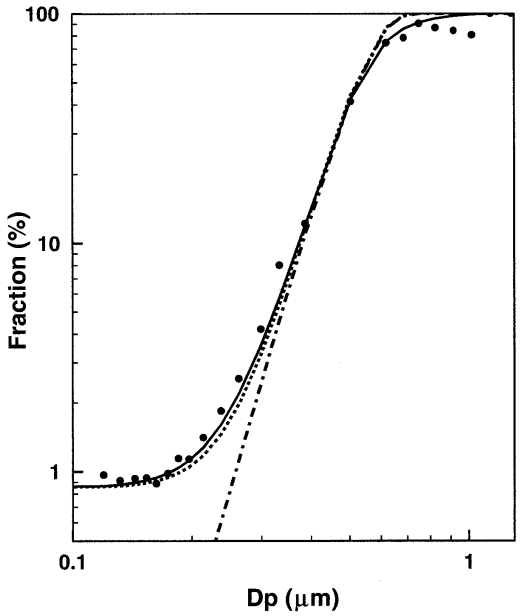

FIG. 7. Fraction of ambient particles included in the crystals as a function of particle size (dots). The solid line is a fit to the data according to Eq. (2). The dash-dotted line is Eq. (11) of DeMott et al. (1994), and the dotted line is a modified version of that equation as explained in the text.

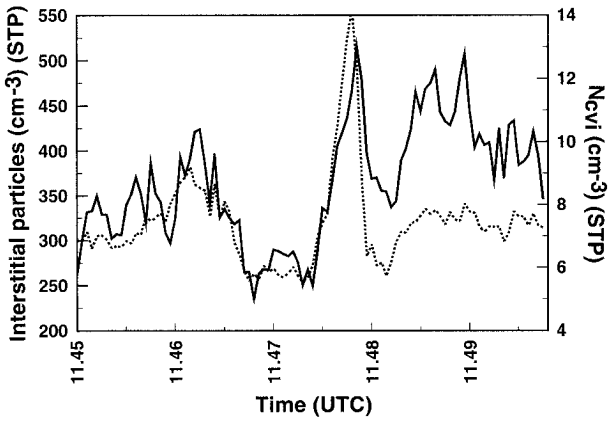

FIG. 8. An example of the covariation of crystal and interstitial aerosol concentration from a segment taken from the flight made on 18 March 1994.

it act on a longer timescale will give a similar result as using a higher RH_w. At sizes larger than 0.33 μm, the agreement is very good. Below this size the two curves diverge. However, by adding a constant factor of 0.0085 to the parameterized nucleation curve as in Eq. (1) (dotted line in Fig. 7), the fit to the data is excellent ($r^2 = 0.9989$). Thus, to explain the data one would need to find a mechanism that gives a finite ($<1\%$) probability for small particles to form ice crystals. The probability curve is valid for ammonium sulfate, but the chemical composition of the aerosol during these measurements is not known. One could speculate that increasing acidity at small sizes or a heterogeneous effect from the presence of small inclusions might alter the shape of this curve.

Recently, several authors (e.g., Jensen and Toon 1994; Sassen et al. 1995) have emphasized the question of a link between the number of aerosol particles in the free troposphere and tropopause region and the life cycle of cirrus clouds. Observations from this study give a mixed picture regarding this question. The interstitial aerosol number concentration varied greatly, but in general it increased from about 250 cm^{-3} at 8200 m to about 1000 cm^{-3} at 8800 m. But as mentioned above, the crystal concentration decreased with height; thus there is an anticorrelation between crystal and aerosol concentration when the data is viewed in this way. Studying individual time series, however, gives another picture. For parts of the cloud where conditions seem to be more homogeneous in terms of potential temperature and aerosol concentration, there is a clear correlation between the number of crystals and aerosol particles. An example of this is presented in Fig. 8. It is important to note that this correlation is not always present and it is possible to find periods where there is a negative correlation as well. This question will be returned to in the next section.

b. Statistics over four flights

The three flights on 22 and 25 March were not suitable for a detailed study similar to that of 18 March because the flight legs were much shorter and not along the horizontal wind component. However, since the weather situations were similar and we believe that these clouds also belong to the category of young cirrus, the data from all the flights were combined in order to present statistics for all flights. Only CVI data from straight and level flight segments are included in this analysis. To exclude periods when the cloud could be directly influenced by aircraft emissions, data points where the ambient interstitial number concentrations exceed 4000 cm^{-3} were not included in the data analysis. The number 4000 cm^{-3} was chosen after ranking the interstitial number concentration from all the flights and looking for the point where the values increased sharply. Furthermore, only in-cloud data points are included in the data analyses, defined as an ambient crystal concentration greater than 3 L^{-1} as measured by the CVI. At this concentration the counting error for the CVI is 25%–30% depending on flow settings. The ensemble of 3-s averages contains a total of 2336 data points. Of those data points, the flight on 18 March represents 16%. The ambient temperatures for this data set ranged between $-35°$ and $-60°$C.

On average, the vertical wind in cloudy air, presented in Fig. 9, had no preferred direction. The bulk of the observations falls within ± 0.35 m s^{-1} of zero, and the maximum values are less than 1 m s^{-1}. Hence, the average vertical wind derived from modeled large-scale

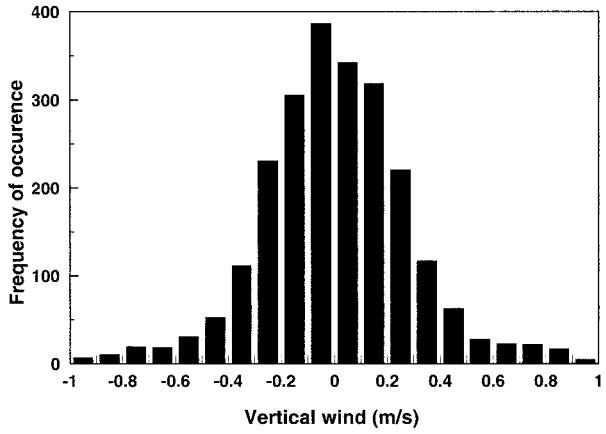

FIG. 9. Frequency distribution of the observed vertical wind in cirrus clouds from four flights.

fields is perhaps not optimum for cloud parameterizations considering that a cloud may form in upwardly moving air and remain in downward-moving air. On grid scales of most numerical models, the average vertical wind may be insignificant or even negative when there may be actually cloud formation within the grid. For subgrid processes in GCMs, Donner et al. (1995) pointed out the need to recognize the scale on which the microphysical parameterization is done, since this significantly affects the resulting cloud properties. In the case of 18 March, the standard deviation of vertical velocity (in the cloudy air) as a function of horizontal scale was about 20 cm s^{-1} for averaging scales between 0.5 and 10 km, and then dropped to 13 cm s^{-1} at 50 km and 5 cm s^{-1} at 100 km. This illustrates how the variance of the vertical wind depends on the horizontal scale over which the wind average is made.

The frequency distribution of RH_w values (not shown) presents a clustering of data points near water saturation with a median of 90%. The 25th and 75th percentiles were 78% and 99%, respectively. It should be mentioned that a 3-s average for the CR-1 instrument is too short compared to its response time for the instrument at the given ambient temperatures. The instrument overshoots and oscillates around the true value at cold temperatures and when exposed to sudden changes in humidity, as can be seen in Figs. 2 and 3. This is a likely cause for observed RH_w values above water saturation. In wave clouds, Heymsfield and Miloshevich (1993) also observed RH_w values around water saturation. However, the vertical wind in these clouds was an order of magnitude larger than the observations presented here. With the estimated uncertainty presented above, it is possible that the humidity data is overestimated by as much as 10% on average.

The observed values of CWC and crystal concentration displayed variations over several orders of magnitude, as can be seen from the probability plot in Fig. 10. Median values of 2.6 cm^{-3} and 6 mg m^{-3} serve as typical concentrations. Sassen et al. (1995) reported ''abnormal'' crystal concentrations (0.6 cm^{-3}, ambient concentration) from in situ observations over Kansas in 1992, which could be attributed to enhanced ambient CCN concentration due to volcanic debris from Mt. Pinatubo entering the troposphere from the stratosphere in tropopause folding events. These crystal concentrations are similar to those reported by Ström and Heintzenberg (1994) from measurements conducted over the European Alps in January 1992. Interestingly, residual particles ($d > 0.5$ μm) from crystals sampled during that campaign showed a chemical signature consistent with volcanic debris from Mt. Pinatubo (Heinzenberg et al. 1996). But in view of the measurements presented here and those reported by Noone et al. (1993) and Ström and Heintzenberg (1994), crystal concentrations on the order of 1 cm^{-3} should probably not be termed abnormal. It is true that reported

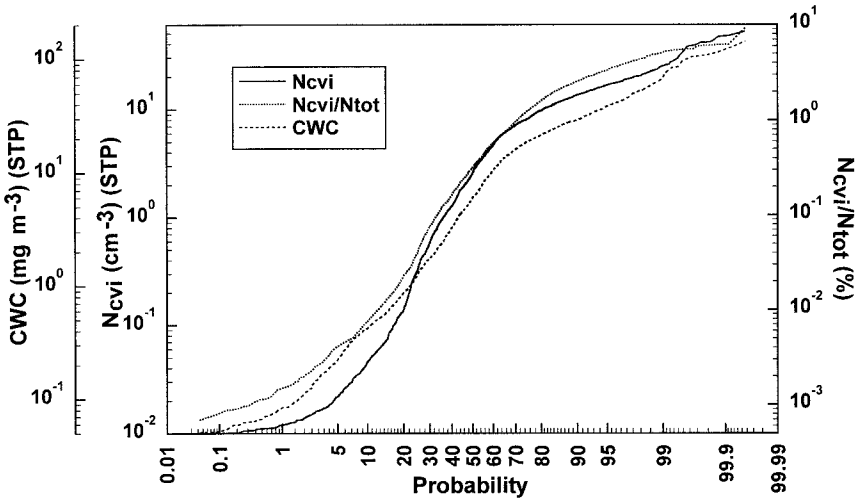

FIG. 10. Probability plots of cloud water content, crystal concentration, and number scavenging ratio as measured by the CVI from four flights.

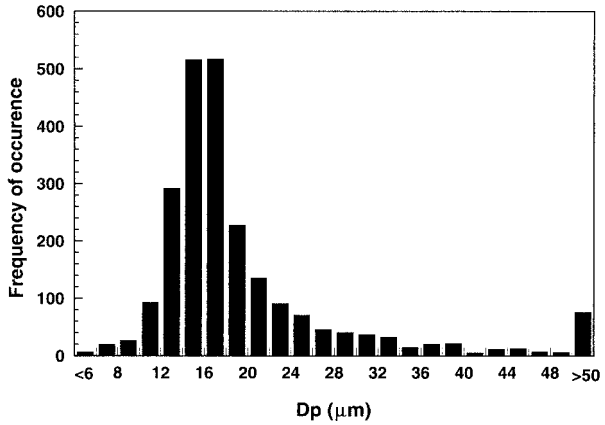

FIG. 11. Frequency distribution of diameter of mean mass from four flights.

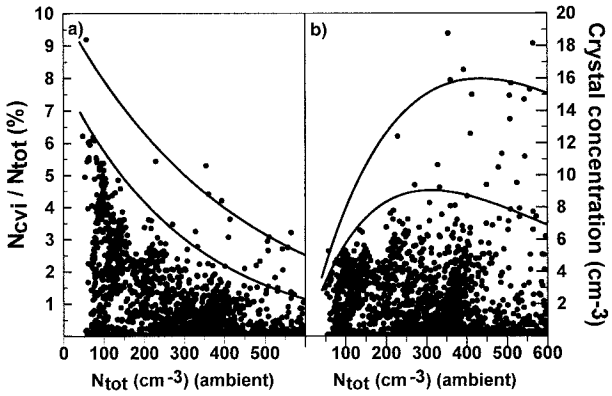

FIG. 12. Scavenging ratio and crystal concentration as a function of aerosol concentration from four flights. See text for a description of the lines in the figure.

observations of high crystal concentrations are few, but this could well be due to the limitations in the measuring techniques commonly used.

Cloud water content and crystal concentrations usually covaried in time, as can be seen in Figs. 2 and 3, and from the frequency distribution of DMM in Fig. 11. The DMM distribution exhibits a narrow mode at 16-μm diameter and is skewed toward larger sizes, and the narrow frequency distribution infers a proportionality between CWC and crystal concentration. From a series of nine measurement flights in cirrus using the FSSP and 2D probes, Moss (1994) showed empirically that for DMM values less than about 35 μm, the DMM was a factor of about 1.5 times the effective diameter. Applying this relationship to our data, the effective diameter should typically be in the 10-μm range; a value that fits well with the replicator data from 18 March. Several other modeling studies, remote sensing, and in situ measurements suggest the presence of crystals sizes typically smaller than 30–40-μm diameter in cirrus (Platt and Spinhirne 1989; Sassen 1991; Kinne et al. 1992; Minnis et al. 1993). J. Coakley (1994, personal communication) also found, by using a bispectral retrieval method (Lin and Coakley 1993), that the effective diameter typically ranged between 10- and 30-μm diameter in single-layered nonopaque clouds. We note that, in cold ice fogs, number mean crystal sizes are smaller than 10-μm diameter and observed size distribution are similar to the distributions presented in Fig. 4 (Ohtake 1970).

In the case study in the previous section, size distributions for the residual aerosol was presented, which appeared to have a number mode around 0.1 μm. However, the particles incorporated in the cloud elements represent only a small fraction of the total aerosol as can be seen in Fig. 10. This number scavenging efficiency, which has a median value of 0.32%, appears to reach a maximum near 10% for this dataset. However, it is difficult to determine how this ratio is related to the number of ambient aerosols. In other words, what is the largest fraction scavenged or number of crystals nucleated for a given aerosol concentration?

Several different clustering patterns of data points can be seen in Fig. 12. Depending on how different curve fits are performed, different relations can be obtained, as is also illustrated in Fig. 12. On the left-hand side of Fig. 12a, the scavenging ratio is plotted as a function of the ambient aerosol concentration. The two curves drawn in Fig. 12 indicate what could be regarded as an upper limit to the scavenging efficiencies as subjectively judged from the data. On the right-hand side of Fig. 12b, the same data and curve fits are shown but for crystal concentration as a function of ambient aerosol concentration. The curves on the right suggest a maximum around 400 cm^{-3}, which in principal makes sense when regarding the measuring limitations of only sampling crystals larger than 4.5 μm. At one extreme, with decreasing aerosol concentration the crystal concentration approaches zero. Even with a nucleation efficiency of 100%, only one crystal can originate from one aerosol particle, neglecting secondary processes like splintering of freezing drops. At the other extreme, the number of crystals would increase (not necessarily linear) with an increasing number of aerosol particles, but at some point one would reach the situation when there is not enough water vapor available to produce more crystals having a size larger than 4.5 μm (cut size of the CVI).

The form of the curves in Fig. 12b suggests that the crystal concentration would be most sensitive for variations in the aerosol concentration up to about 300 cm^{-3}. At the same time the highest crystal concentrations are found for aerosol concentrations above 300 cm^{-3}. One should keep in mind that it is possible, or perhaps even likely, that the dataset is not completely free from effects by aircraft emissions. Diluted contrails, which are difficult to distinguish from the natural cloud, can be embedded in the cirrus fields. As an example, the three peaks between 1152 and 1153 UTC in Fig. 3a are likely to be embedded contrails. However, due to the corresponding large peaks in the aerosol concentration, the

data from this period were excluded from the analyses in this section. On other occasions, it may be difficult to screen the data from direct effects by aircraft emissions. The high-altitude clouds over continental Europe could also be affected indirectly by an increased aerosol burden from air traffic near the tropopause region. Perhaps there have never been cirrus cloud measurements over Europe free from anthropogenic influences.

From ground-based measurements of microphysical and aerosol properties using the CVI, Anderson et al. (1994) studied how aerosol perturbations may modulate the droplet number concentration and mean size. Similar to this study the authors observed a close correlation between the cloud water content and cloud particle concentration but were unable to find an unambiguous relation between the droplet and aerosol number concentration. They explained this by turbulence causing inhomogeneities in the cloud such that each data point is actually a mixture of cloudy and noncloudy air. Thus, the variance in their observed concentrations are governed mainly by dynamical processes rather than microphysical processes. Mixing and entrainment are features that may mask the modulation of cloud element concentration by changes in aerosol number.

It is evidently difficult to establish the link between the number of aerosols and the crystal concentration in cirrus clouds. The main reason for this is that the signal sought after is much smaller than the natural variability, as it is in many atmospheric problems. Clearly, as presented in Figs. 2 and 3, cirrus cloud microphysics respond much more strongly to dynamic forcing than to variations in ambient aerosol number concentration. However, it is possible that changes in aerosol properties will alter the average properties of cirrus clouds. As predicted by models, this may not be a linear response (e.g., Heymsfield and Sabin 1989), but even a small change in cloud properties may be of significance for the climate.

Further research will be needed to establish clearly the relationship between these two properties. The measurements presented herein, which come from a relatively polluted region of the upper troposphere, would be useful for comparison with cirrus measurements in cleaner regions and for constraining modeling studies of cirrus perturbation by anthropogenic aerosol. There is also a general observational need to quantify the anthropogenic enhancement of aerosol in the upper troposphere.

4. Summary and conclusions

The measurements presented here show large numbers of small crystals ($D < 30$ μm), data that add to the growing body of evidence that cirrus clouds can contain high-number concentration of crystals at sizes below the detection limits of traditional optical probes (e.g. Platt and Spinhirne 1989; Noone et al. 1993). Median values of crystal concentration and cloud water content observed in four clouds were 2.6 cm^{-3} and 6 mg m^{-3} (STP), respectively.

Aerosol particles below 0.3-μm diameter were found to dominate the number concentration of crystal residue particles, even though they were scavenged with low efficiency. These small particles clearly play an important role in cirrus formation. For aerosol particles larger than 0.3 μm, the slope of the scavenging efficiency can be explained by calculated nucleation probabilities for haze droplets formed on ammonium sulfate aerosols. For smaller sizes the calculated curve underestimates the number of scavenged aerosols, which could be due to a change of the chemical composition of the aerosol. The high relative humidities near water saturation, residual aerosol size distribution, and droxtal-shaped crystals observed in the clouds support the idea that the most important nucleation process in cold cirrus is the freezing of haze droplets. Clearly small aerosol particles ($\sim$0.1-μm diameter) must be included in any conceptual model of cirrus formation; however, accurate quantification will require more information about aerosol chemical composition and how this affects crystal nucleation.

The variations in crystal concentration, cloud water content, and air parcel vertical displacement (as indicated by both potential temperature and vertical wind measurements) suggest that the dynamic forcing for the cloud on 18 March was due to wave structures having a period close to the calculated Brunt–Väisälä frequency. The vertical displacement experienced by an air parcel relative to the unperturbed air appeared to be only 25–50 m. This result gives new insight into the link between dynamic and microphysical processes and could be used to constrain explicit microphysical models.

The crystal habits, crystal size distributions, and residual particle size distributions all show striking similarities to observations made in ice fogs at low temperatures (near -40°C). In both cases the crystals shapes are droxtals (amorphous spheres), the crystal number distribution peaks at diameters below 10 μm, and the residue particle number distribution peaks at diameters below 0.5 μm. Moreover, ice fogs display aerosol scavenging efficiencies by number comparable to values reported in this study. These observations raise the possibility that formation processes in cirrus clouds and ice fogs may be similar.

Occasionally, the time series of crystal concentration shows a positive correlation with the ambient aerosol concentration. However, overall the dataset shows the difficulty of making an empirical assessment of this relationship from observation in a single region and time. Future studies using these measurements to compare with cirrus observations in cleaner regions and/or to constrain explicit microphysical models of cirrus formation would be useful.

Acknowledgments. We acknowledge the flight facility at DLR for excellent collaboration. We thank Dr. Kevin Noone and Dr. Keith Bigg for helpful discussions and comments on the manuscript. This work was possible through the support by NFR (Swedish Natural Science

Research Council). Tad Anderson acknowledges support from the International Meteorological Institute at Stockholm University, the International Program of US/NFS, and US/NOAA/NA67RJ0155.

REFERENCES

Anderson, T. L., R. J. Charlson, and D. S. Covert, 1993: Calibration of a counterflow virtual impactor at aerodynamic diameters from 1 to 15μm. *Aerosol Sci. Technol.,* **19,** 317–329.

——, D. S. Covert, and R. J. Charlson, 1994: Cloud droplet number studies with a counterflow virtual impactor. *J. Geophys. Res.,* **99,** 8249–8256.

Busen, R., and A. L. Buck, 1993: A high performance hygrometer for aircraft use: Description, installation, and flight data. Institut für Physik der Atmosphäre Rep. 10, 29 pp. [Available from Institut für Physik der atmosphäre, Oberpfaffenhofen, D-82234 Weβling, Germany.]

DeMott, P. J., M. P. Meyers, and W. R. Cotton, 1994: Parameterization and impact of ice initiation processes relevant to numerical model simulations of cirrus clouds. *J. Atmos. Sci.,* **51,** 77–90.

Donner, L. J., J. Warren, and J. Ström, 1995: Implementing microphysics at physically appropriate scales in GCMs. *Proc. Workshop on Cloud Microphysics Parameterizations in Global Atmospheric Circulation Models,* Alberta, Canada, World Meteor. Org., 133–140.

Dye, J. E., and D. Baumgardner, 1984: Evaluation of the forward scattering spectrometer probe. Part I: Electronic and optical studies. *J. Atmos. Oceanic Technol.,* **1,** 329–344.

Hallett, J., 1976: Measurements of size, concentration and structure of atmospheric particulates by the airborne continous replicator. Air Force Geophysics Laboratory, Final Rep., Contract AFGL-TR-76-0149, 92 pp. [Available from B. Strauss, DLR, Institute für Physik der Atmosphäre, Oberpfaffenhofer D-82234 Weßling, Germany.]

Heintzenberg, J., K. Okada, and J. Ström, 1996: On the composition of non-volatile material in upper tropospheric aerosols and cirrus crystals. *Atmos. Res.,* **41,** 81–88.

Heymsfield, A. J., and R. M. Sabin, 1989: Cirrus crystal nucleation by homogeneous freezing of solution droplets. *J. Atmos Sci.,* **46,** 2252–2264.

——, and L. M. Miloshevich, 1993: Homogeneous ice nucleation and supercooled liquid water in orographic wave clouds. *J. Atmos. Sci.,* **50,** 2335–2353.

——, and ——, 1995: Relative humidity and temperature influences on cirrus formation and evolution: Observations from wave clouds and FIRE II *J. Atmos. Sci.,* **52,** 4302–4326.

Jensen, E. J., and O. B. Toon, 1994: Ice nucleation in the upper troposphere: Sensitivity to aerosol number density, temperature, and cooling rate. *Geophys. Res. Lett.,* **21,** 2019–2022.

——, ——, D. L. Westphal, S. Kinne, and A. J. Heymsfield, 1994: Microphysical modeling of cirrus 1. Comparison with 1986 FIRE IFO measurements. *J. Geophys. Res.,* **99,** 10 421–10 442.

Knollenberg, R. G., 1970: The optical array: An alternative to scattering or extinction for airborne particle size determination. *J. Appl. Meteor.,* **9,** 86–103.

Kinne, S., T. P. Ackerman, A. J. Heymsfield, F. P. J. Valero, K. Sassen, and J. D. Spinhirne, 1992: Cirrus microphysical and radiative transfer: Cloud field study on 28 October 1986. *Mon. Wea. Rev.,* **120,** 661–684.

Lin, H., and J. Heintzenberg, 1995: A theoretical study of the counterflow virtual impactor. *J. Aerosol Sci.,* **26,** 903–914.

Lin, X., and J. A. Coakley, 1993: Retrieval of properties for semi-transparent clouds from multispectral infrared imagenary data. *J. Geophys. Res.,* **98,** 18 501–18 514.

Minnis, P., P. W. Heck, and D. F. Young, 1993: Inference of cirrus cloud properties using satellite-observed visible and infrared radiances. Part II: Verification of theoretical cirrus radiative properties. *J. Atmos. Sci.,* **50,** 1305–1322.

Moss, S. J., 1994: Calculation of the effective radius of ice particles in cirrus clouds using the C-130 microphysical measurements from EUCREX'93. *Proc. Seventh Workshop, European Cloud Radiation Experiment,* Villeneuve d'Ascq, France, European Union, 22–26.

Noone, K. J., J. A. Ogren, J. Heintzenberg, R. J. Charlson, and D. S. Covert, 1988: Design and calibration of a counterflow virtual impactor for sampling of atmospheric fog and cloud droplets. *Aerosol Sci. Technol.,* **8,** 235–244.

——, ——, A. Hallberg, J. Heintzenberg, J. Ström, H.-C. Hansson, B. Svenningsson, A. Wiedensohler, S. Fuzzi, C. Facchini, B. G. Arends, and A. Berner, 1992: Changes in aerosol size- and phase distribution due to physical and chemical processes in fog. *Tellus,* **44B,** 489–504.

——, ——, J. Heintzenberg, J. Ström, and J. A. Ogren, 1993: In situ observations of cirrus cloud microphysical properties using the counterflow virtual impactor. *J. Atmos. Oceanic Technol.,* **10,** 294–303.

Ogren, J. A., J. Heintzenberg, and R. J. Charlson, 1985: In-situ sampling of clouds with a droplet to aerosol converter. *Geophys. Res. Lett.,* **12,** 121–303.

Ohtake, T., 1970: Unusual crystal in ice fog. *J. Atmos. Sci.,* **27,** 509–511.

——, 1970: Studies on ice fog. Geophysical Institute, University of Alaska Rep. UAG R-211, 177 pp. [Available from J. Ström, Dept. of Meteorology, Stockholm University, S-106 91 Stockholm, Sweden.]

Platt, C. M. R., and J. D. Spinhirne, 1989: Optical and microphysical properties of cold cirrus cloud: Evidence for regions of small ice particles. *J. Geophys. Res.,* **94,** 11 151–11 164.

Sassen, K., 1991: Corona-producing cirrus cloud properties derived from polarization lidar and photographic analyses. *Appl. Opt.,* **30,** 3421–3428.

——, D. O'C. Starr, and T. Uttal, 1989: Mesoscale and microscale structures of cirrus clouds: Three case studies. *J. Atmos. Sci.,* **46,** 372–396.

——, and Coauthors, 1995: The 5–6 December 1991 FIRE IFO II jet stream cirrus case study: Possible influences of volcanic aerosols. *J. Atmos. Sci.,* **52,** 97–123.

Schröder, F., and J. Ström, 1997: Aircraft measurements of sub micrometer aerosol particles (<7nm) in the midlatitude free troposphere and tropopause region. *Atmos. Res.,* **44,** 333–356.

Schumann, U., P. Konopka, R. Baumann, R. Busen, T. Gerz, H. Schlager, P. Schulte, and H. Volkert, 1995: Estimate of diffusion parameters of aircraft exhaust plumes near the tropopause from nitric oxide and turbulence measurements. *J. Geophys. Res.,* **100,** 14 147–14 162.

Stephens, G. L., S.-C. Tsay, P. W. Stackhouse Jr., and P. J. Flatau, 1990: The relevance of microphysical and radiative properties of cirrus clouds to climate and climatic feedback. *J. Atmos. Sci.,* **47,** 1742–1753.

Ström, J., and J. Heintzenberg, 1994: Water vapor, condensed water and crystal concentration in orographically influenced cirrus clouds. *J. Atmos. Sci.,* **51,** 2368–2383.

——, R. Busen, M. Quante, B. Guillemet, P. R. A. Brown, and J. Heintzenberg, 1994a: Pre-EUCREX Intercomparison of airborne humidity measuring instruments, *J. Atmos. Oceanic Technol.,* **11,** 1392–1399.

——, J. Heintzenberg, K. J. Noone, K. B. Noone, J. A. Ogren, F. Albers, and M. Quante, 1994b: Small crystals in cirrus clouds: Their residue sized distribution, cloud water content and related cloud properties. *J. Atmos Res.,* **32,** 125–141.

Thuman, W. C., and E. Robinson, 1954: Studies of Alaskan ice-fog particles. *J. Meteor.,* **11,** 151–156.

Twohy, C. H., A. D., Clarke, S. G. Warren, L. F. Radke, and R. J. Charlson, 1989: Light absorbing material extracted from cloud droplets and its effect on cloud albedo. *J. Geophys. Res.,* **94,** 8623–8631.

Zuber, A., and G. Witt, 1987: Optical hygrometer using differential absorption of hydrogen Lyman–Alpha radiation. *Appl. Opt.,* **26,** 3083–3089.